

# How to link theory and experiment for single-chain magnets beyond the Ising model: magnetic properties modeled from *ab initio* calculations of molecular fragments

Michael Böhme and Winfried Plass

## Electronic Supplementary Information (ESI)

### Contents

1	Comparison of coupling schemes	S2
2	Extrapolation of the correlation length	S3
3	Correlation length and coupling schemes	S4
4	Magnetic susceptibility of a 1D periodic Ising chain	S6
5	<i>Ab initio</i> computational models and single-ion properties	S7
6	Fit of the magnetic susceptibility	S14
7	Determined magnetic coupling constants $J_{\text{calc}}$	S17
8	Spin states in dependence on the single-ion anisotropy	S18
9	Additional POLY_ANISO results	S19
10	Extrapolation of the magnetic susceptibility	S21
11	Magnetic interchain interactions	S22
12	Basis set information	S25
13	Decomposition of the calculated magnetic susceptibility	S26

## 1 Comparison of coupling schemes

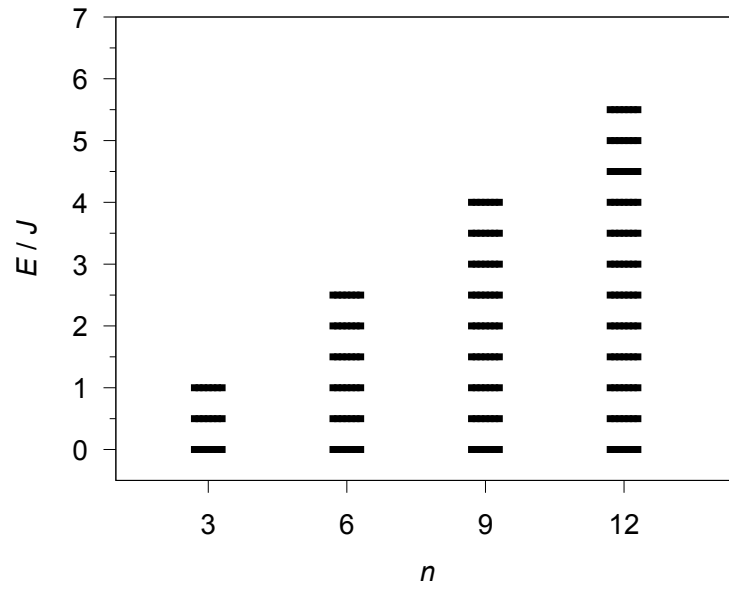


**Fig. S1:** Energy spectrum scaled in units of  $J$  for an  $n$ -membered open chain as obtained from the Hamiltonian given in eqn (1) from the main manuscript for selected model sizes  $n$ .

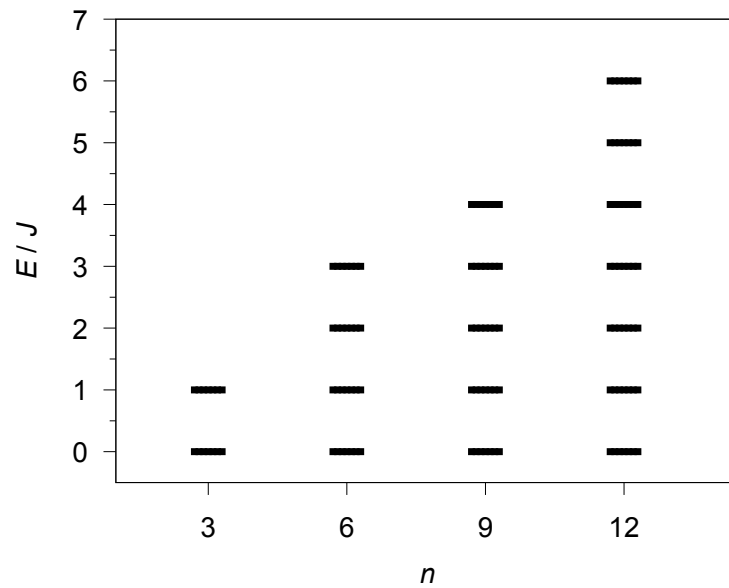


**Fig. S2:** Energy spectrum scaled in units of  $J$  for an  $n$ -membered spin ring as obtained from the Hamiltonian given in eqn (2) from the main manuscript for selected model sizes  $n$ .

## 2 Extrapolation of the correlation length

The correlation length  $2\tilde{\zeta}$  for a 1D periodic chain of Ising-type spins ( $S_{\text{eff}} = 1/2$ ) is defined as in eqn (4) of the main manuscript. By assuming the correlation function  $\gamma$  for an Ising spin as given in eqn (3), one can show that the correlation lengths  $2\tilde{\zeta}_{\text{chain}}(n)$  and  $2\tilde{\zeta}_{\text{ring}}(n)$  as given in eqns (5) and (6) of the main manuscript are identical to eqn (4) for  $n \rightarrow \infty$ .

$$\lim_{n \rightarrow \infty} 2\tilde{\zeta}_{\text{chain}}(n) = \frac{1 + \gamma}{1 - \gamma} - \underbrace{\frac{2\gamma}{n} \frac{1 - \gamma^n}{(1 - \gamma)^2}}_{=0} = \exp\left(\frac{J}{2k_{\text{B}}T}\right) \quad (\text{S1})$$

$$\lim_{n \rightarrow \infty} 2\tilde{\zeta}_{\text{ring}}(n) = \frac{1 + \gamma}{1 - \gamma} \cdot \underbrace{\frac{1 - \gamma^n}{1 + \gamma^n}}_{=1} = \exp\left(\frac{J}{2k_{\text{B}}T}\right) \quad (\text{S2})$$

### 3 Correlation length and coupling schemes

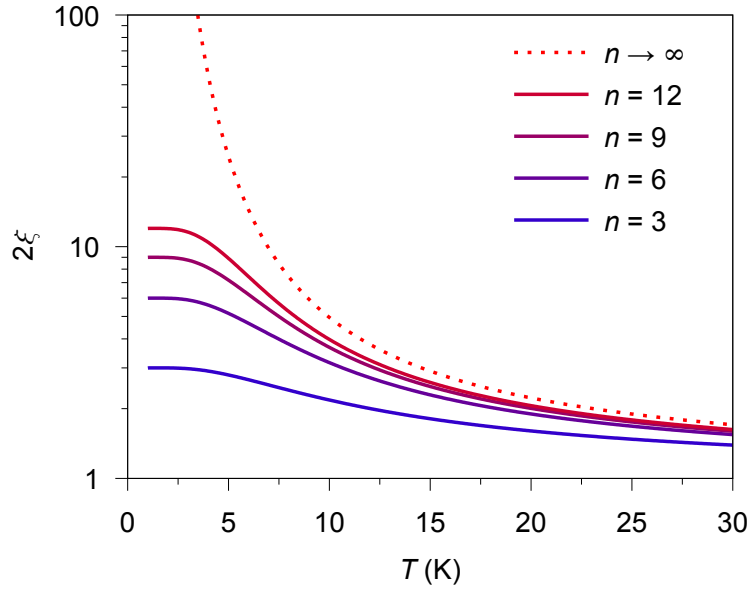


**Fig. S3:** Temperature dependence of the correlation length  $2\bar{\xi}_{\text{chain}}$  for selected  $n$ -membered open chains of spins as obtained from eqn (5) from the main manuscript for Ising-type spins ( $J/k_B = 32$  K). The dotted line shows the extrapolation ( $n \rightarrow \infty$ ) for a 1D periodic chain ( $2\bar{\xi}_{\infty}$ ).

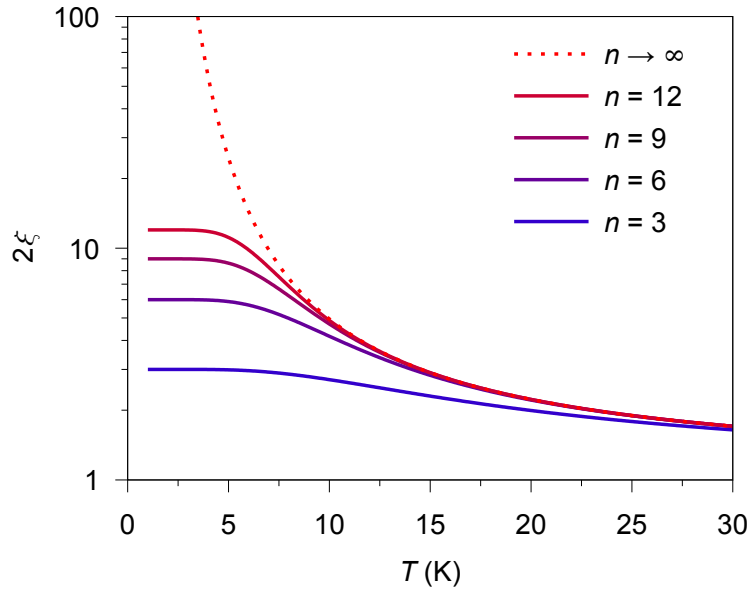


**Fig. S4:** Temperature dependence of the correlation length  $2\bar{\xi}_{\text{ring}}$  for selected  $n$ -membered spin rings as obtained from eqn (6) from the main manuscript for Ising-type spins ( $J/k_B = 32$  K). The dotted line shows the extrapolation ( $n \rightarrow \infty$ ) for a 1D periodic chain ( $2\bar{\xi}_{\infty}$ ).

**Table S1:** Temperature dependence of the correlation length  $2\zeta$  for a 1D periodic chain ( $2\zeta_\infty$ ) and the two different coupling schemes ( $2\zeta_{\text{chain}}(n = 12)$ : 12-membered open chain;  $2\zeta_{\text{ring}}(n = 12)$ : 12-membered spin ring) as obtained from eqns (4)–(6) from the main manuscript for Ising-type spins and assuming a ferromagnetic exchange interaction ( $J/k_B = 32$  K).  $\gamma$  represents the correlation function for Ising spins as given in eqn (3) from the main manuscript.

$T$ (in K)	$\gamma$	$2\zeta_\infty$	$2\zeta_{\text{chain}}(n = 12)$	$2\zeta_{\text{ring}}(n = 12)$
5	0.92167	24.53	8.90	11.13
10	0.66404	4.95	3.98	4.88
15	0.48792	2.91	2.60	2.90
20	0.37995	2.23	2.06	2.23
25	0.30951	1.90	1.79	1.90
30	0.26052	1.70	1.63	1.70
35	0.22467	1.58	1.52	1.58
40	0.19738	1.49	1.44	1.49
45	0.17593	1.43	1.38	1.43
50	0.15865	1.38	1.34	1.38
55	0.14444	1.34	1.30	1.34
60	0.13255	1.31	1.28	1.31
65	0.12246	1.28	1.25	1.28
70	0.11379	1.26	1.23	1.26
75	0.10626	1.24	1.22	1.24
80	0.09967	1.22	1.20	1.22
85	0.09384	1.21	1.19	1.21
90	0.08866	1.19	1.18	1.19
95	0.08401	1.18	1.17	1.18
100	0.07983	1.17	1.16	1.17

#### 4 Magnetic susceptibility of a 1D periodic Ising chain

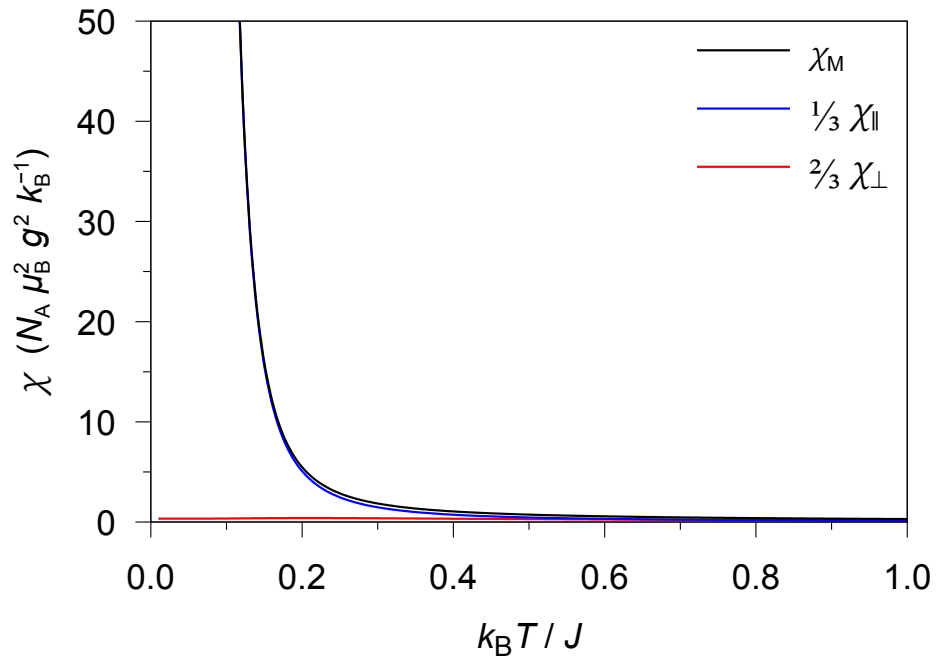


**Fig. S5:** Magnetic susceptibility  $\chi$  (in  $N_A \mu_B^2 g^2 k_B^{-1}$ ) for a 1D periodic Ising chain (black line;  $S_{\text{eff}} = 1/2$ ;  $J/k_B = 32$  K) as obtained by eqns (8)–(10) from the main manuscript. The molar magnetic susceptibility  $\chi_M$  can be decomposed into two parts with respect to the orientation of the spins: parallel ( $1/3 \chi_{||}$ ; blue line) and perpendicular ( $2/3 \chi_{\perp}$ ; red line).

## 5 *Ab initio* computational models and single-ion properties

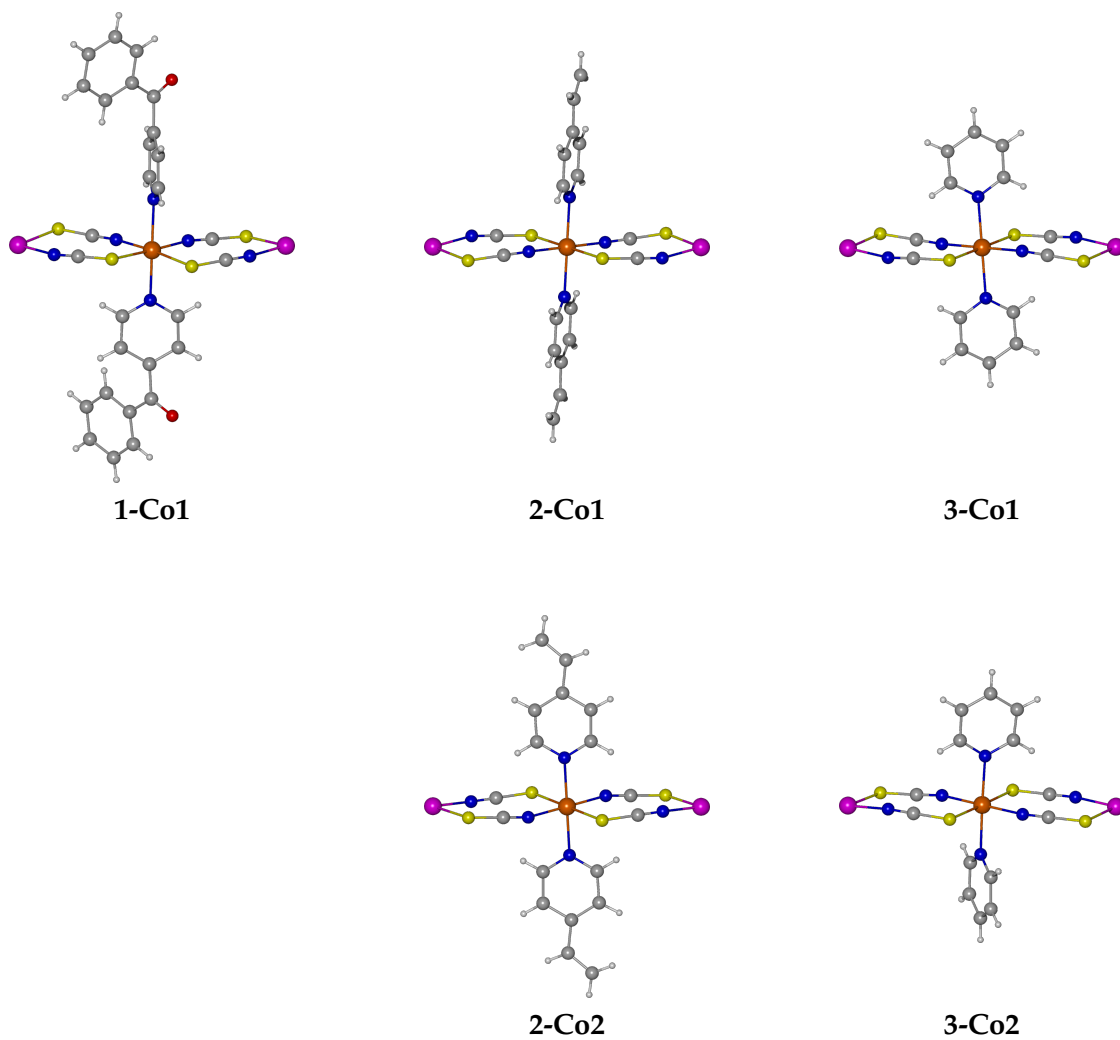


**Fig. S6:** *Ab initio* computational models for the crystallographically independent cobalt(II) centers in 1-3 (color code: Co – orange; Zn – pink).

**Table S2:** Relative CASSCF energies (in  $\text{cm}^{-1}$ ) of all quartet and the nine lowest doublet states for the mononuclear cobalt(II) computational models.

$2S + 1$	Term	Subterm	1-Co1	2-Co1	2-Co2	3-Co1	3-Co2		
4	${}^4F$	${}^4T_{1g}$	0	0	0	0	0		
			115	770	588	475	155		
			919	1265	1155	998	870		
		${}^4T_{2g}$	6994	5780	5590	5382	5380		
			7157	8236	7916	7608	7600		
			7695	8756	8936	8532	8502		
		${}^4A_{2g}$	15379	15882	15850	15259	15367		
			${}^4P$	${}^4T_{1g}$	21052	21318	21488	21390	21257
					23702	23250	22696	22270	22423
	24212	26275			26529	26188	25927		
	2	${}^2G$	12697	11986	11742	12024	11801		
			14754	15987	16039	16121	15727		
19101			18071	17595	17728	17660			
19129			18519	18501	18532	18424			
19199			19413	19210	19147	19071			
20315			20101	20068	20078	19801			
20414			21036	20957	20808	20642			
20482			21495	21401	21273	21166			
24619			24351	24354	24299	24181			

**Table S3:** Relative CASPT2 energies (in  $\text{cm}^{-1}$ ) of all quartet and the nine lowest doublet states for the mononuclear cobalt(II) computational models.

$2S + 1$	Term	Subterm	1-Co1	2-Co1	2-Co2	3-Co1	3-Co2	
4	${}^4F$	${}^4T_{1g}$	0	0	0	0	0	
			114	807	647	506	241	
			860	1148	1030	853	844	
		${}^4T_{2g}$	7629	6808	6597	6344	6509	
			7764	9370	8982	8623	8789	
			8971	9798	9980	9516	9659	
	${}^4P$	${}^4A_{2g}$	17578	18030	18035	17355	17618	
			${}^4T_{1g}$	18522	18793	18996	18863	18867
				21190	21190	20564	20035	20385
		21738		24064	24375	23975	23820	
		2	${}^2G$	9955	9276	9018	9318	9225
				12128	13194	13270	13373	13079
16686	15909			15543	15705	15764		
16471	16462			16389	16403	16433		
16625	16789			16589	16547	16596		
17613	17347			17324	17361	17187		
17080	18341			18242	18108	18074		
17920	18614			18535	18459	18448		
20882	20771			20650	21114	20732		

**Table S4:** Relative RASSI-SO energies (in  $\text{cm}^{-1}$ ) of the  ${}^4\text{T}_{1g}[\text{}^4\text{F}]$  ground multiplet for the mononuclear cobalt(II) computational models.

Kramers doublet	1-Co1	2-Co1	2-Co2	3-Co1	3-Co2
1	0	0	0	0	0
2	257	139	153	182	243
3	487	888	787	707	538
4	800	1127	1022	969	866
5	1392	1466	1391	1290	1311
6	1420	1576	1497	1391	1396

**Table S5:** Calculated zero-field splitting parameters and their Cartesian components of the  $g$  tensor ( $S_{\text{eff}} = 3/2$ ) for the mononuclear cobalt(II) computational models.

	1-Co1	2-Co1	2-Co2	3-Co1	3-Co2
$D$ ( $\text{cm}^{-1}$ )	114.18	63.86	73.64	89.15	109.50
$E$ ( $\text{cm}^{-1}$ )	33.74	15.59	24.55	10.65	30.71
$E/D$	0.30	0.24	0.33	0.12	0.28
$g_x$	1.722	2.743	2.745	2.811	1.801
$g_y$	2.002	2.435	2.527	2.623	2.222
$g_z$	3.130	2.000	1.947	1.869	3.072

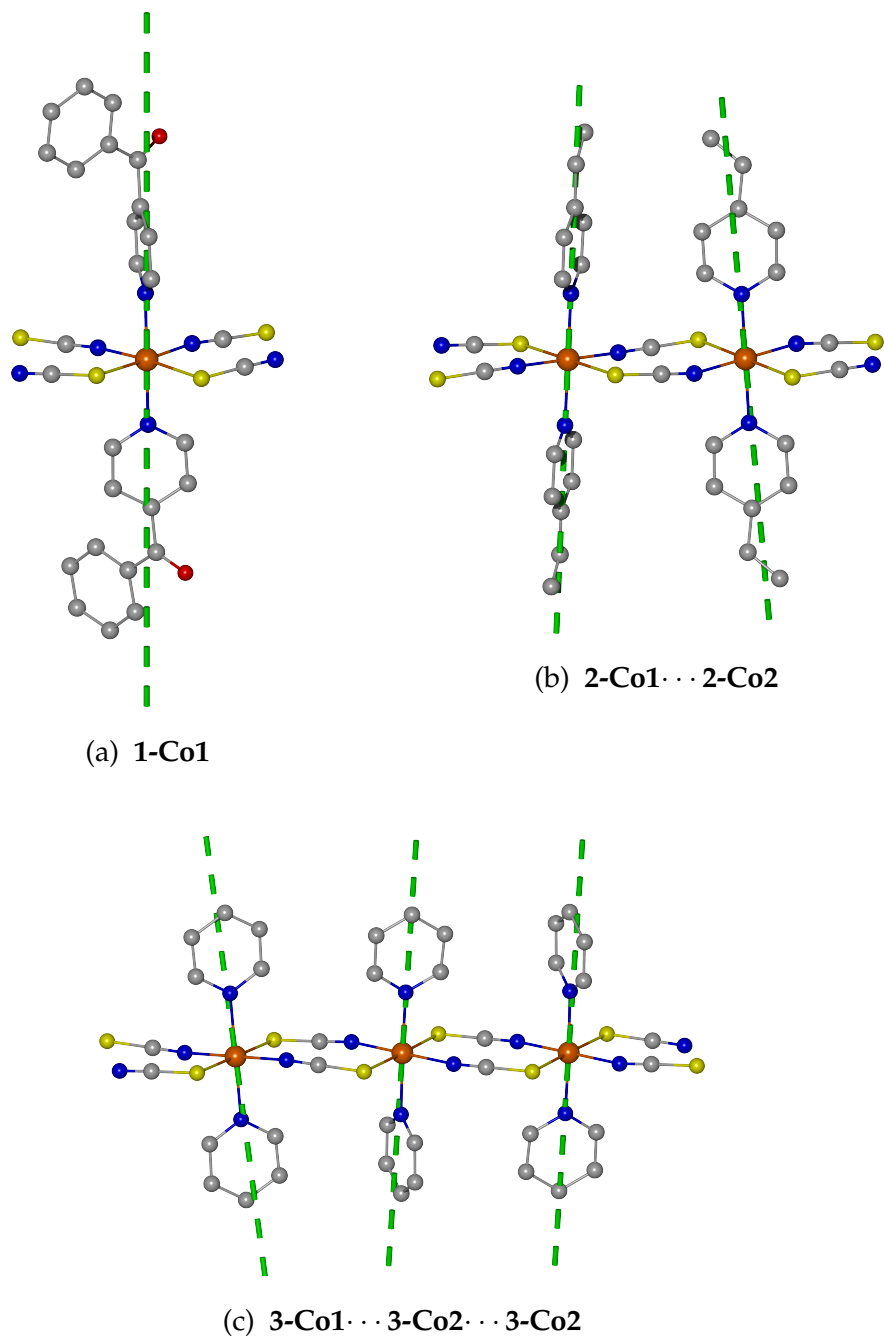
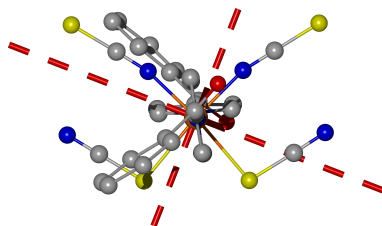
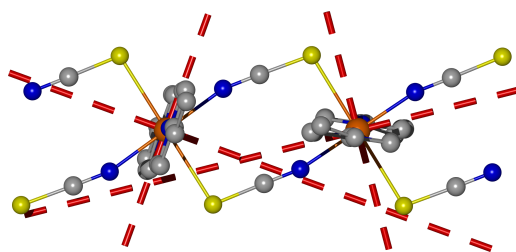


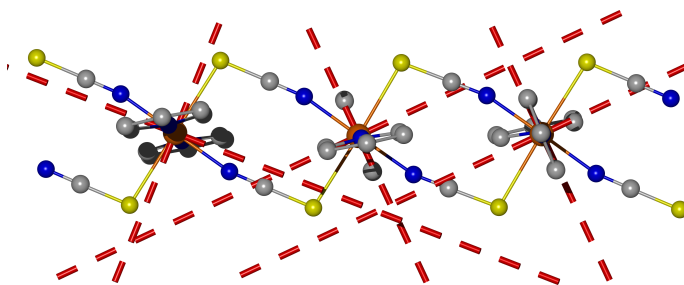
**Fig. S7:** Easy-axis of magnetization from *ab initio* calculations of the ground state KD ( $S_{\text{eff}} = 1/2$ ) for the individual centers projected onto the smallest repeating sequence of the chain structures for 1–3. Hydrogen atoms have been omitted for clarity.



(a) 1-Co1



(b) 2-Co1...2-Co2



(c) 3-Co1...3-Co2...3-Co2

**Fig. S8:** Hard-axes of magnetization from *ab initio* calculations of the ground state KD ( $S_{\text{eff}} = 1/2$ ) for the individual centers projected onto the smallest repeating sequence of the chain structures for 1–3 from a top view. Hydrogen atoms have been omitted for clarity.

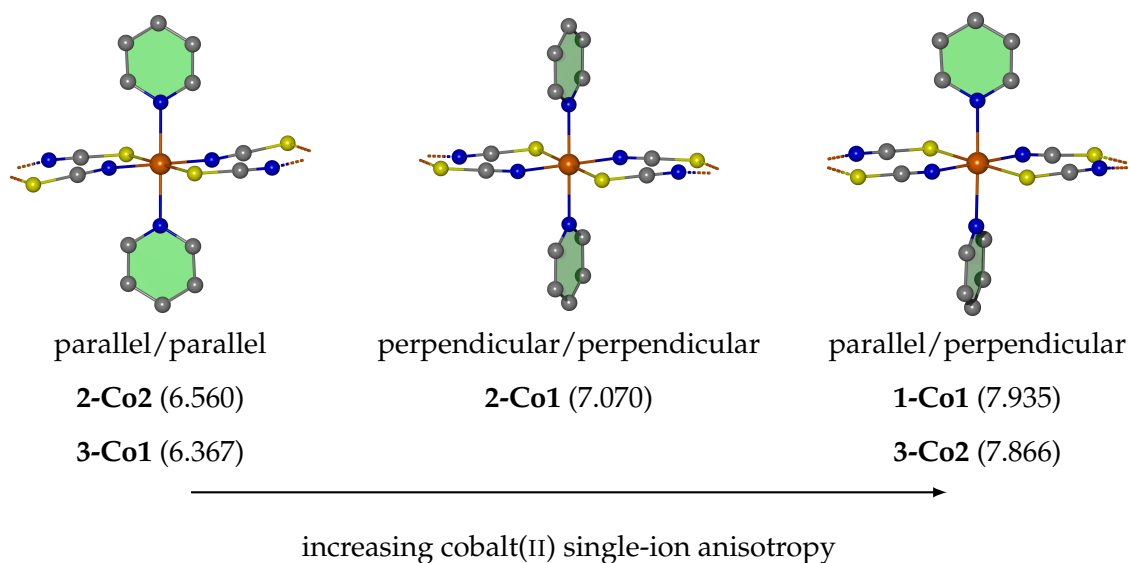


**Fig. S9:** Classification of the crystallographically independent cobalt(II) centers of **1–3** in three groups depending on the orientation of the  $\pi$ -planes (in green) of both pyridine-based co-ligands with respect to the direction of the thiocyanate chain (hydrogen atoms have been omitted for clarity). The values in the parentheses are the corresponding Cartesian  $g_z$  values of the ground state KD.

## 6 Fit of the magnetic susceptibility

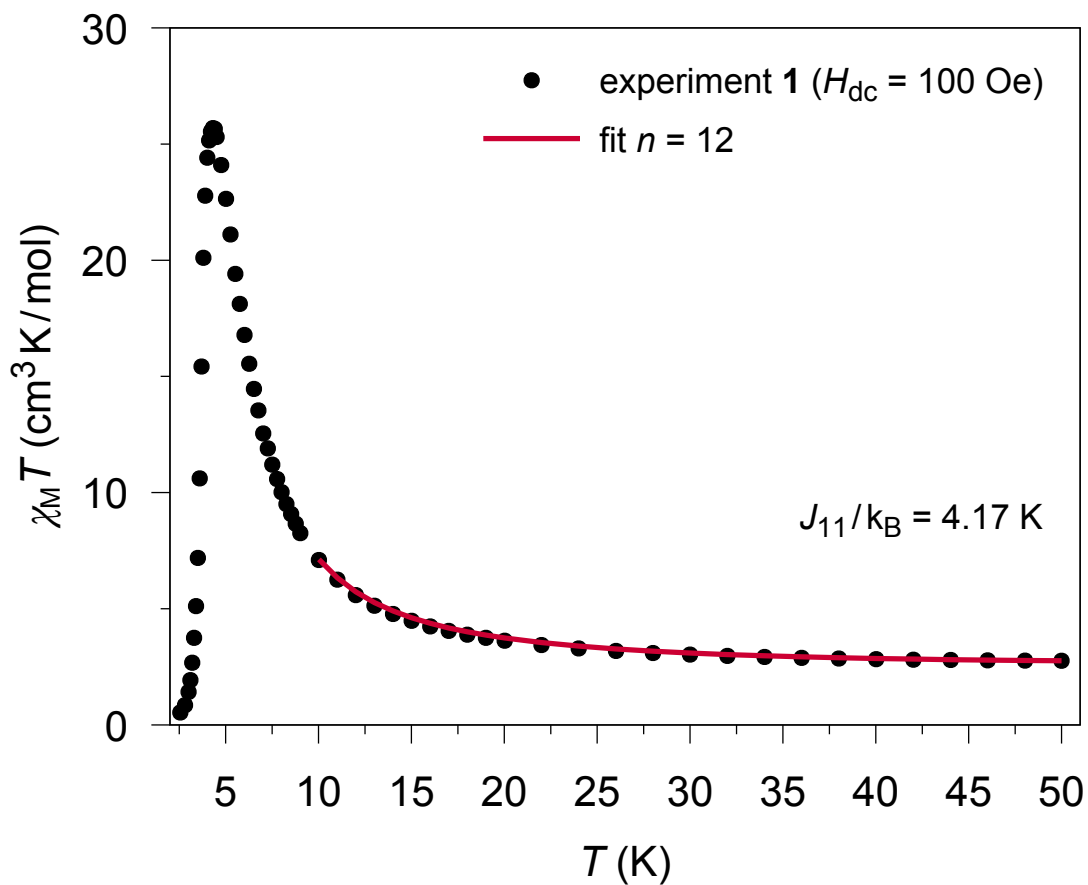


**Fig. S10:** Experimental and simulated temperature dependence of  $\chi_M T$  (•) for 1. The POLY\_ANISO program on basis of the *ab initio* calculations was used to simulate the magnetic susceptibility employing a 12-membered spin ring coupling scheme in the temperature range of  $10\text{ K} \leq T \leq 50\text{ K}$ . The root-mean-square deviation between the experimental and theoretical magnetic susceptibility was minimized by adjusting the theoretical coupling constant  $J_{11}$  between the individual centers. The red line shows the best fit of the magnetic susceptibility based on the *ab initio* calculations.

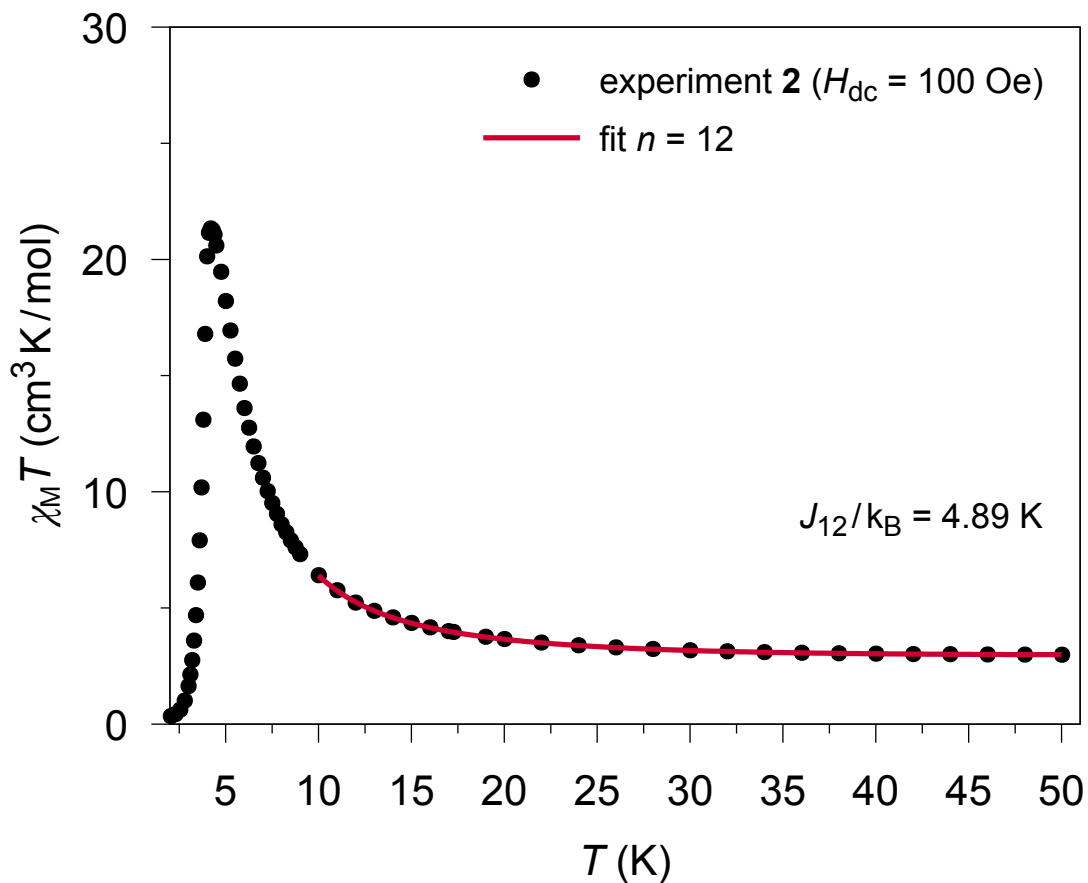


**Fig. S11:** Experimental and simulated temperature dependence of  $\chi_M T$  (•) for **2**. The POLY\_ANISO program on basis of the *ab initio* calculations was used to simulate the magnetic susceptibility employing a 12-membered spin ring coupling scheme in the temperature range of  $10\text{ K} \leq T \leq 50\text{ K}$ . The root-mean-square deviation between the experimental and theoretical magnetic susceptibility was minimized by adjusting the theoretical coupling constant  $J_{12}$  between the individual centers. The red line shows the best fit of the magnetic susceptibility based on the *ab initio* calculations.

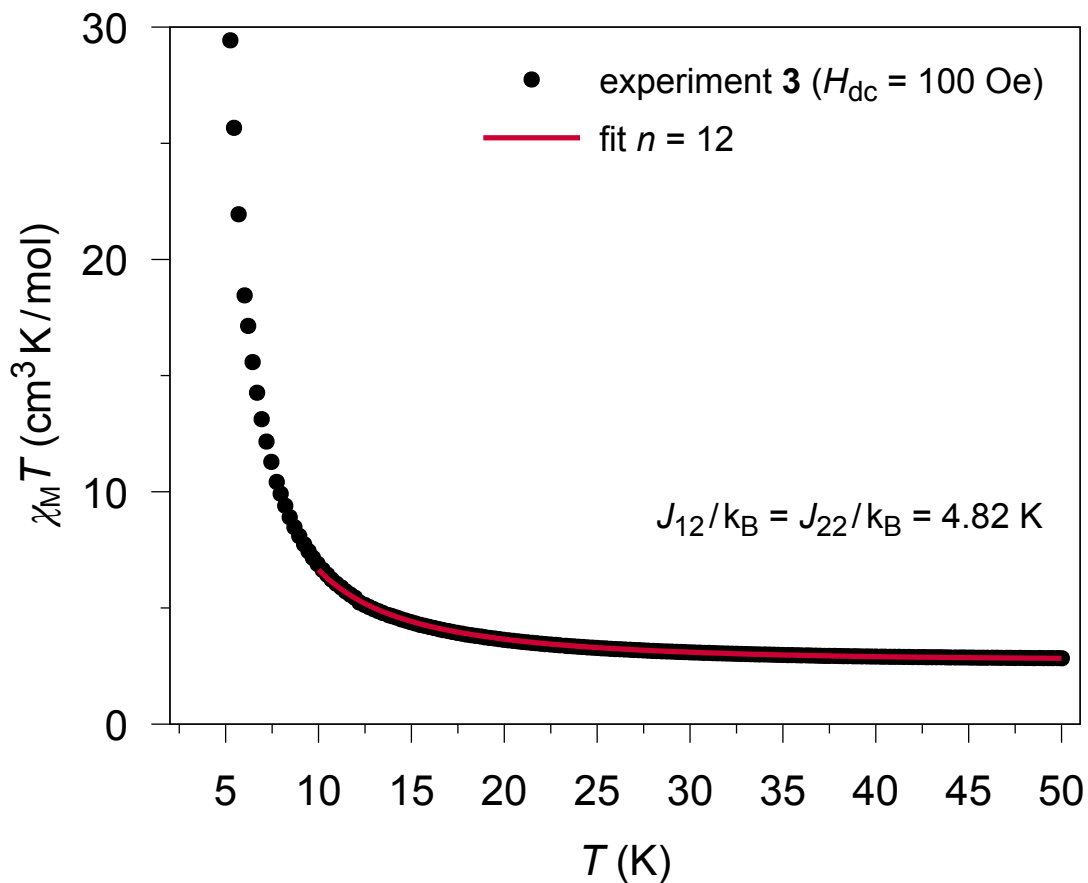


**Fig. S12:** Experimental and simulated temperature dependence of  $\chi_M T$  (•) for **3**. The POLY\_ANISO program on basis of the *ab initio* calculations was used to simulate the magnetic susceptibility employing a 12-membered spin ring coupling scheme in the temperature range of  $10\text{ K} \leq T \leq 50\text{ K}$ . The root-mean-square deviation between the experimental and theoretical magnetic susceptibility was minimized by adjusting the theoretical coupling constants  $J_{12}$  ( $\equiv J_{22}$ ) between the individual centers. The red line shows the best fit of the magnetic susceptibility based on the *ab initio* calculations.

## 7 Determined magnetic coupling constants $J_{\text{calc}}$

**Table S6:** Coupling constants (in K) for 1–3 and four hypothetical chains (**2-Co1**, **2-Co2**, **3-Co1**, **3-Co2**) as obtained from the simulation of 12-membered spin rings employing the POLY\_ANISO program on the base of *ab initio* fragment calculations and the fitted coupling constants of the Lines model  $J_{ij}$ .

Compound	Simulated system	$J_{\text{calc}}/k_{\text{B}}$	$J_{\text{calc}}/k_{\text{B}}$	$J/k_{\text{B}}$
		eqn (13)	eqn (14)	exp.
<b>1</b>	$[\cdots\mathbf{1-Co1}\cdots]_{12}$	28.8	29.2	32(2)
<b>2</b>	$[\cdots\mathbf{2-Co1}\cdots\mathbf{2-Co2}\cdots]_6$	28.5	29.6	27(3)
<b>3</b>	$[\cdots\mathbf{3-Co1}\cdots\mathbf{3-Co2}\cdots\mathbf{3-Co2}\cdots]_4$	29.0	29.8	29(2)
Hypothetical chains				
<b>2-Co1</b>	$[\cdots\mathbf{2-Co1}\cdots]_{12}$	31.4	32.1	–
<b>2-Co2</b>	$[\cdots\mathbf{2-Co2}\cdots]_{12}$	na	28.4	–
<b>3-Co1</b>	$[\cdots\mathbf{3-Co1}\cdots]_{12}$	na	25.9	–
<b>3-Co2</b>	$[\cdots\mathbf{3-Co2}\cdots]_{12}$	32.4	32.9	–

## 8 Spin states in dependence on the single-ion anisotropy

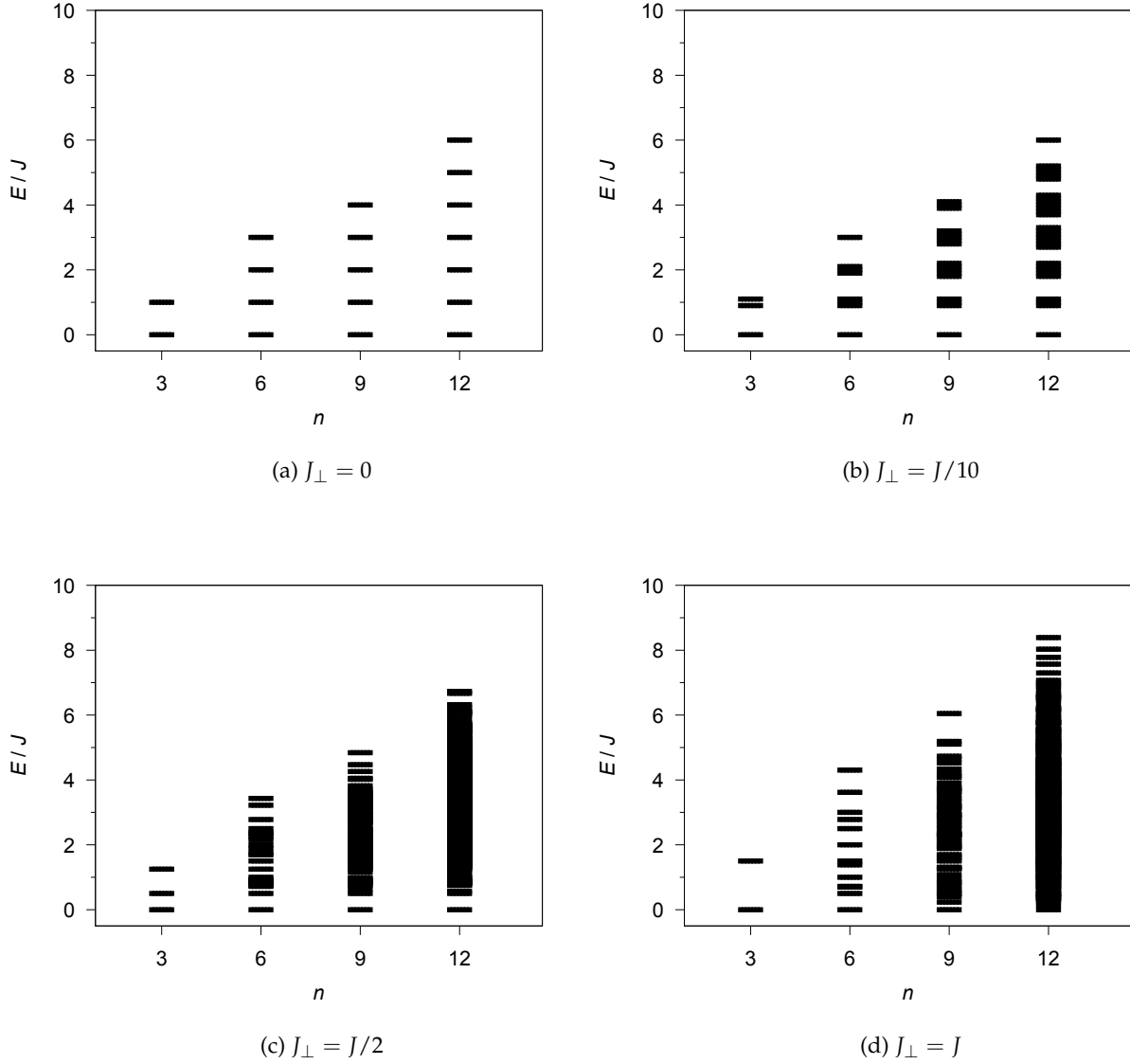


**Fig. S13:** Energy spectrum scaled in units of  $J$  for an  $n$ -membered **spin ring** coupling scheme simulating different spin anisotropies (as obtained by (S3) with  $J_{\parallel} \equiv J$ ): (a) Ising, (b) weak anisotropic Heisenberg, (c) anisotropic Heisenberg, (d) isotropic Heisenberg. The lowering of the anisotropy from (a) to (d) goes together with an overlap of the higher spin multiplets.

$$\begin{aligned}
 \hat{H}_{\text{ring}} = & -J_{\parallel} \left[ S_1^z S_n^z + \sum_{i=1}^{n-1} S_i^z S_{i+1}^z \right] \\
 & - J_{\perp} \left[ S_1^x S_n^x + S_1^y S_n^y + \sum_{i=1}^{n-1} [S_i^x S_{i+1}^x + S_i^y S_{i+1}^y] \right]
 \end{aligned} \tag{S3}$$

## 9 Additional POLY\_ANISO results

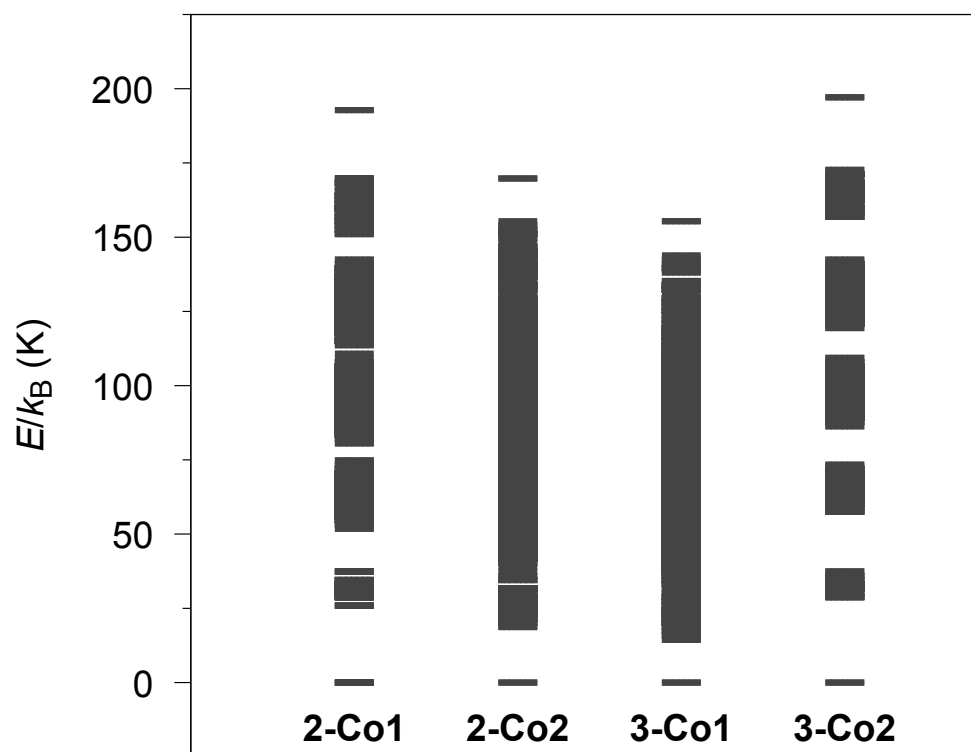


**Fig. S14:** Spin states of hypothetical compounds consisting of only one crystallographically independent spin center (**2-Co1**, **2-Co2**, **3-Co1**, and **3-Co2**) as obtained by the POLY\_ANISO program employing the *ab initio* fragment calculations. A 12-membered spin ring coupling scheme together with the fitted theoretical coupling constants  $J_{ij}$  have been used. The lower single-ion anisotropy in case of **2-Co2** and **3-Co1** goes together with an overlap of the higher spin multiplets (cf. Fig. S13).

**Table S7:** Calculated Cartesian components of the  $\mathbf{g}$  tensor for the ground state doublet in 1–3 employing a 12-membered spin ring coupling scheme ( $S_{\text{eff}} = 1/2$ ;  $g_{\parallel} = g_z/n$  with  $n = 12$ ).

	<b>1</b>	<b>2</b>	<b>3</b>
$n$	12	12	12
Simulated system	$[\cdots \mathbf{1-Co1} \cdots]_{12}$	$[\cdots \mathbf{2-Co1} \cdots \mathbf{2-Co2} \cdots]_6$	$[\cdots \mathbf{3-Co1} \cdots \mathbf{3-Co2} \cdots \mathbf{3-Co2} \cdots]_4$
$g_x$	0.000	0.000	0.000
$g_y$	0.000	0.000	0.000
$g_z$	95.208	81.259	87.854
$g_{\parallel}$	7.934	6.772	7.321

**Table S8:** List of POLY\_ANISO simulations employing a coupling scheme of an  $n$ -membered spin ring for 1–3 used for the extrapolation of magnetic properties. The simulations were performed in a way that takes the correct repeating sequence and ratio of the crystallographically independent cobalt(II) centers into account.

$n$	<b>1</b>	<b>2</b>	<b>3</b>
3	$[\cdots \mathbf{1-Co1} \cdots]_3$		$[\cdots \mathbf{3-Co1} \cdots \mathbf{3-Co2} \cdots \mathbf{3-Co2} \cdots]$
4	$[\cdots \mathbf{1-Co1} \cdots]_4$	$[\cdots \mathbf{2-Co1} \cdots \mathbf{2-Co2} \cdots]_2$	
5	$[\cdots \mathbf{1-Co1} \cdots]_5$		
6	$[\cdots \mathbf{1-Co1} \cdots]_6$	$[\cdots \mathbf{2-Co1} \cdots \mathbf{2-Co2} \cdots]_3$	$[\cdots \mathbf{3-Co1} \cdots \mathbf{3-Co2} \cdots \mathbf{3-Co2} \cdots]_2$
7	$[\cdots \mathbf{1-Co1} \cdots]_7$		
8	$[\cdots \mathbf{1-Co1} \cdots]_8$	$[\cdots \mathbf{2-Co1} \cdots \mathbf{2-Co2} \cdots]_4$	
9	$[\cdots \mathbf{1-Co1} \cdots]_9$		$[\cdots \mathbf{3-Co1} \cdots \mathbf{3-Co2} \cdots \mathbf{3-Co2} \cdots]_3$
10	$[\cdots \mathbf{1-Co1} \cdots]_{10}$	$[\cdots \mathbf{2-Co1} \cdots \mathbf{2-Co2} \cdots]_5$	
11	$[\cdots \mathbf{1-Co1} \cdots]_{11}$		
12	$[\cdots \mathbf{1-Co1} \cdots]_{12}$	$[\cdots \mathbf{2-Co1} \cdots \mathbf{2-Co2} \cdots]_6$	$[\cdots \mathbf{3-Co1} \cdots \mathbf{3-Co2} \cdots \mathbf{3-Co2} \cdots]_4$

## 10 Extrapolation of the magnetic susceptibility

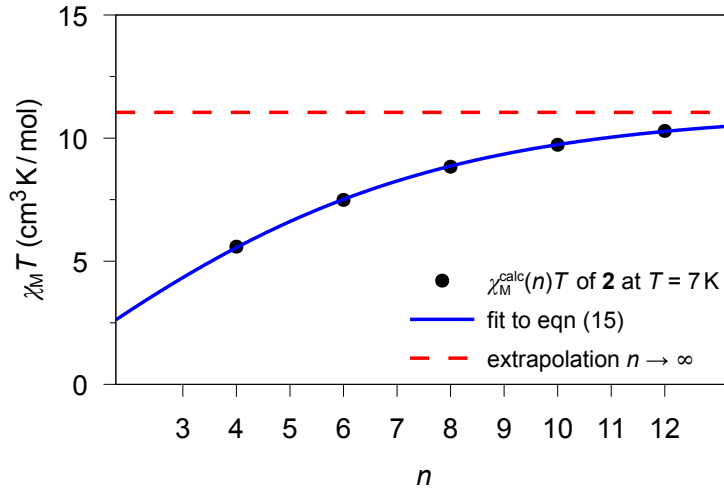


**Fig. S15:** Calculated magnetic susceptibility as  $\chi_M^{\text{calc}}(n)T$  of **2** at  $T = 7$  K for different model sizes  $n$  of an  $n$ -membered **spin ring** employing the theoretical coupling constant  $J_{12}/k_B = 4.89$  K. The blue solid line represents the best fit ( $a = 11.04(5)$  cm<sup>3</sup>K/mol;  $b = 0.7585(20)$ ) according to eqn (15) from the main manuscript and the red dashed line represents the limit for a periodic system ( $n \rightarrow \infty$ ), *i.e.* the parameter  $a$ .

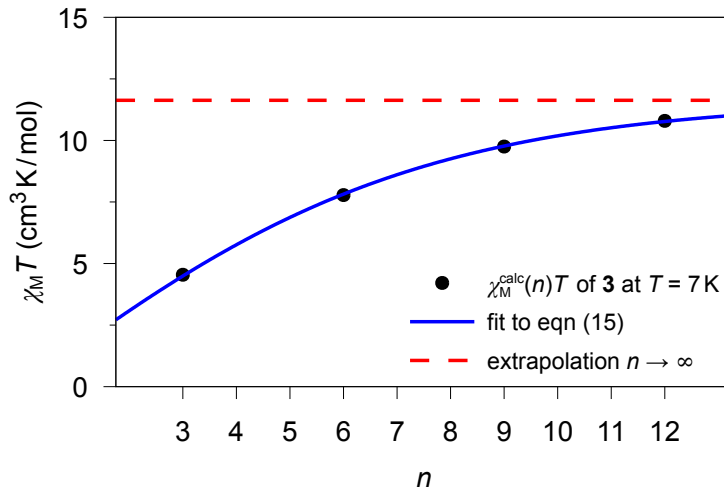


**Fig. S16:** Calculated magnetic susceptibility as  $\chi_M^{\text{calc}}(n)T$  of **3** at  $T = 7$  K for different model sizes  $n$  of an  $n$ -MEMBERED SPIN RING employing the theoretical coupling constant  $J_{12}/k_B \equiv J_{22}/k_B = 4.82$  K. The blue solid line represents the best fit ( $a = 11.63(8)$  cm<sup>3</sup>K/mol;  $b = 0.7621(31)$ ) according to eqn (15) from the main manuscript and the red dashed line represents the limit for a periodic system ( $n \rightarrow \infty$ ), *i.e.* the parameter  $a$ .

## 11 Magnetic interchain interactions

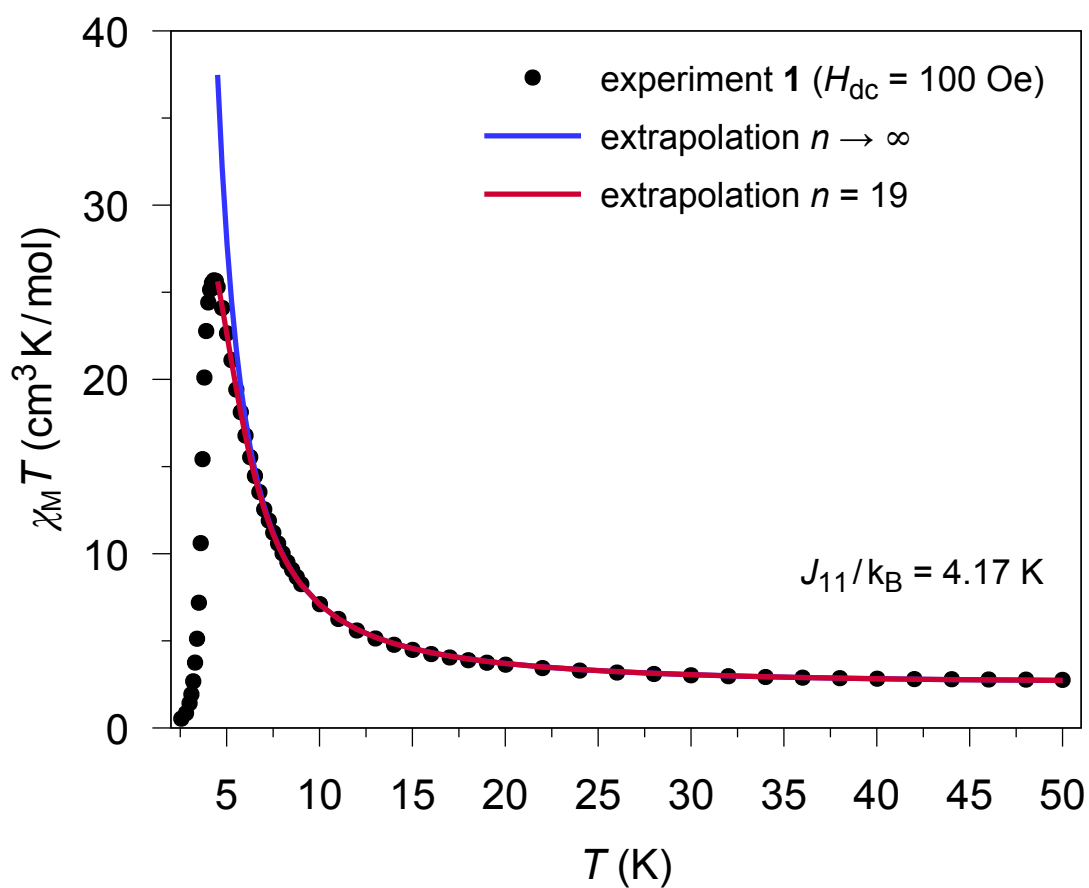


**Fig. S17:** Experimental and simulated temperature dependence of  $\chi_M T$  (•) for **1**. Colored lines represent extrapolations of different sizes of the  $n$ -membered spin ring model (red:  $n = 19$ ; blue:  $n \rightarrow \infty$ ) based on *ab initio* fragment calculations to investigate the low temperature behavior of the magnetic susceptibility ( $4.5 \text{ K} \leq T \leq 50 \text{ K}$ ).

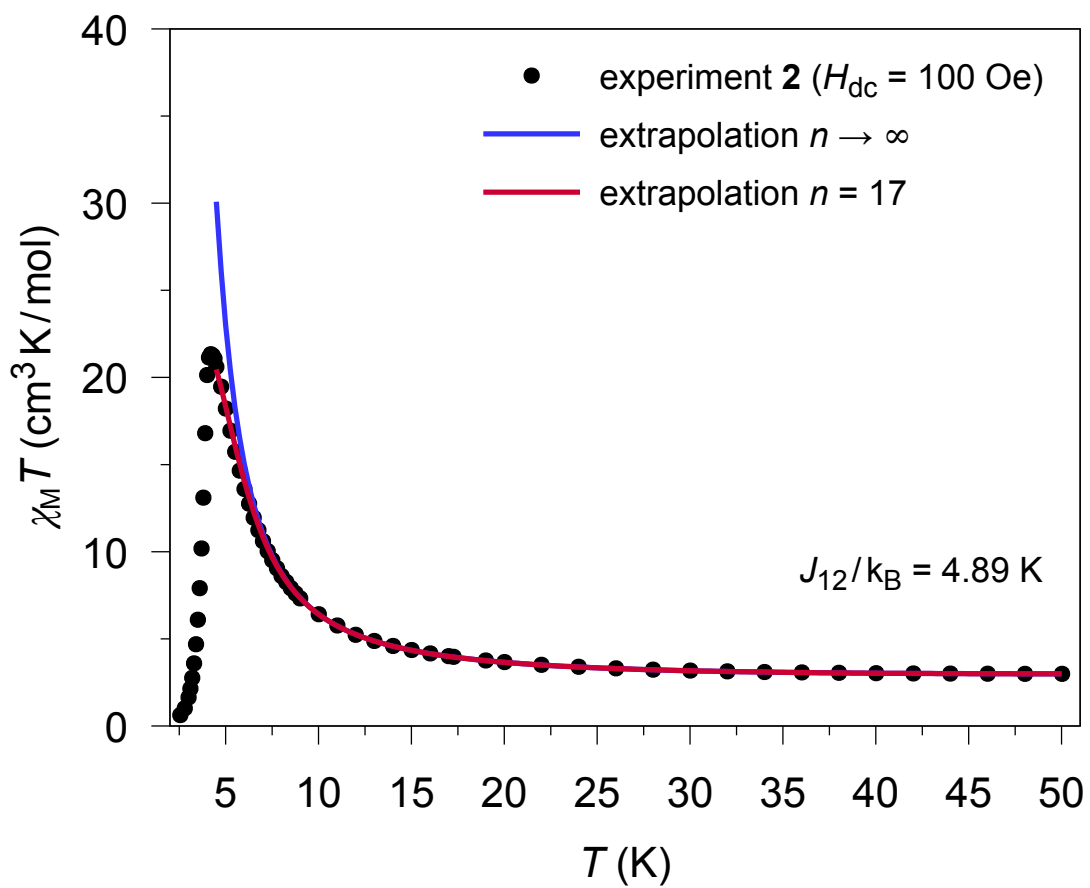


**Fig. S18:** Experimental and simulated temperature dependency of  $\chi_M T$  (●) for **2**. Colored lines represent extrapolations of different sizes of the  $n$ -membered spin ring model (red:  $n = 17$ ; blue:  $n \rightarrow \infty$ ) based on *ab initio* fragment calculations to investigate the low temperature behavior of the magnetic susceptibility ( $4.5 \text{ K} \leq T \leq 50 \text{ K}$ ).

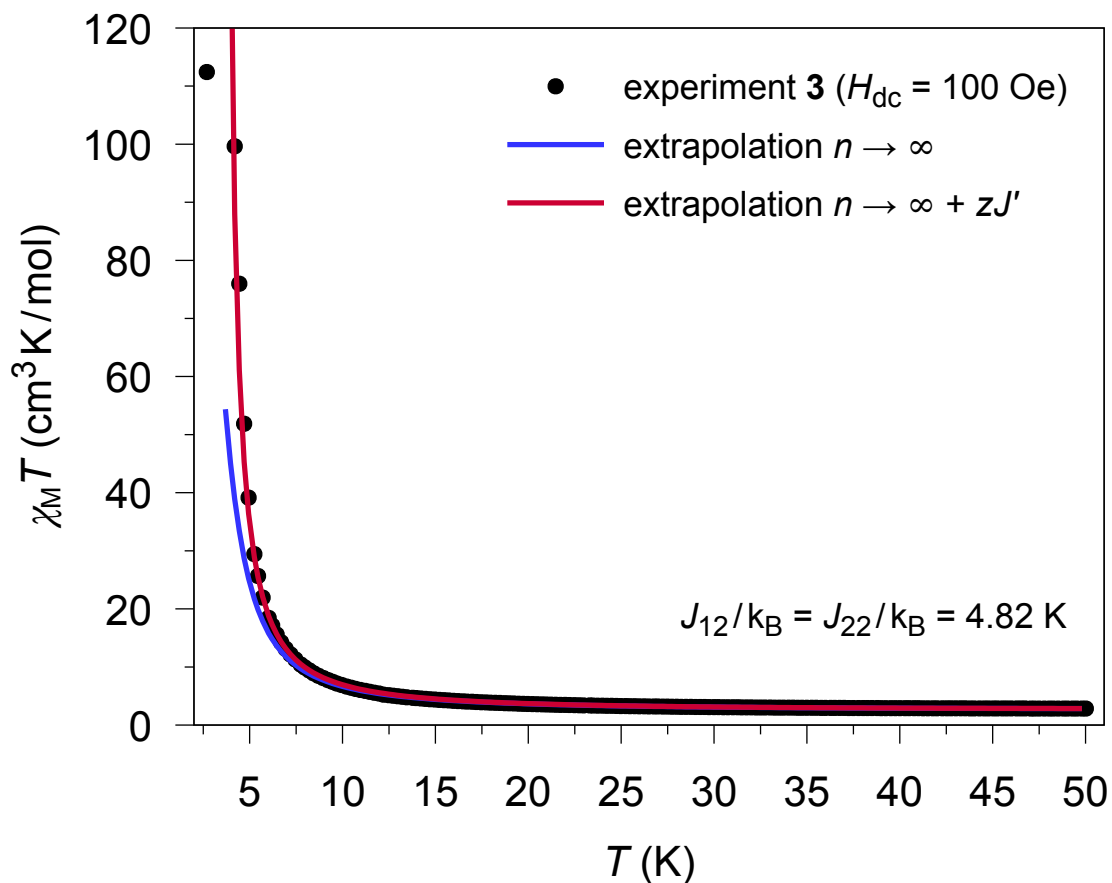


**Fig. S19:** Experimental and simulated temperature dependence of  $\chi_M T$  (•) for **3**. The blue solid line represents an extrapolation  $n \rightarrow \infty$  of the  $n$ -membered spin ring model based on *ab initio* fragment calculations. The red solid line shows the mean-field corrected magnetic susceptibility according to eqn (16) of the main manuscript ( $n \rightarrow \infty$ ;  $zJ'/k_B = 0.85 \text{ K}$ ).

## 12 Basis set information

**Table S9:** Basis sets used for the *ab initio* calculations of 1–3.

Atom	Basis set
Co	Co.ANO-RCC...6s5p4d2f1g.
Zn	Zn.ANO-RCC...5s4p2d.
S (donor)	S.ANO-RCC...5s4p2d1f.
S (non-donor)	S.ANO-RCC...4s3p.
N (donor)	N.ANO-RCC...4s3p2d1f.
N (non-donor)	N.ANO-RCC...3s2p.
O	O.ANO-RCC...3s2p.
C	C.ANO-RCC...3s2p.
H	H.ANO-RCC...2s.

### 13 Decomposition of the calculated magnetic susceptibility

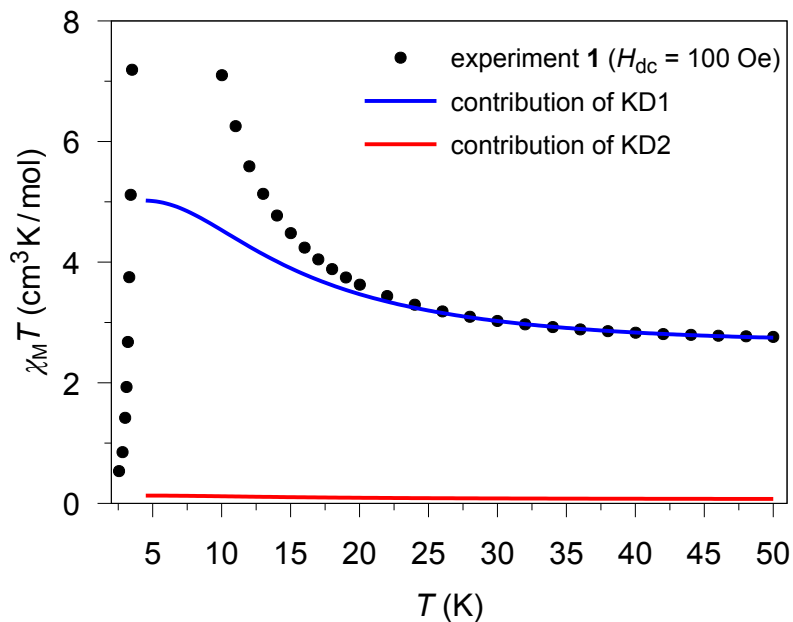


**Fig. S20:** Experimental ( $\bullet$ ) and calculated magnetic susceptibility  $\chi_M^{\text{calc}}(n = 6)T$  of a six-membered spin ring for **1** (colored lines) decomposed into the contribution of the ground state Kramer's doublet (blue line) and first excited Kramer's doublet (red line), respectively. For this simulation the lowest two KDs were taken into account ( $4^6 = 4096$  microstates) instead of the lowest KD ( $2^6 = 64$  microstates;  $J_{11}/k_B = 4.17$  K).

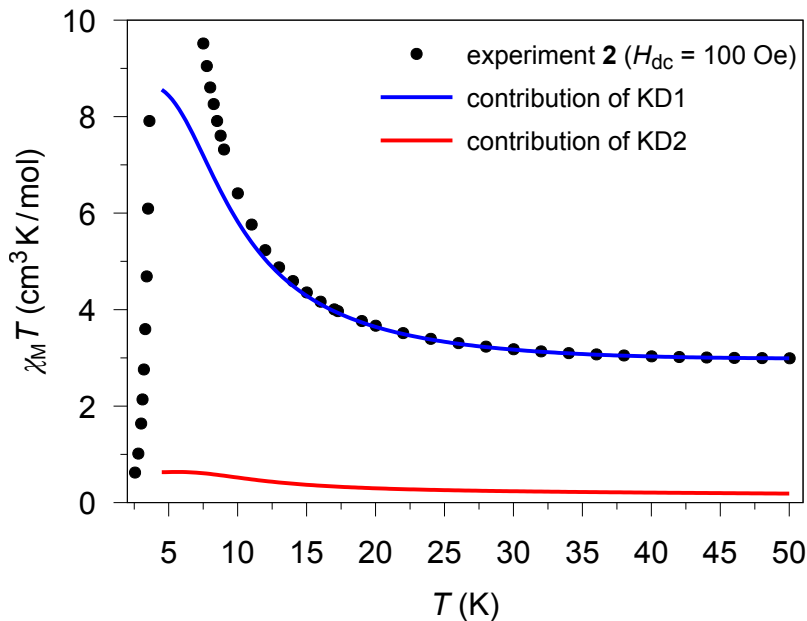


**Fig. S21:** Experimental ( $\bullet$ ) and calculated magnetic susceptibility  $\chi_M^{\text{calc}}(n=6)T$  of a six-membered spin ring for **2** (colored lines) decomposed into the contribution of the ground state Kramers doublet (blue line) and first excited Kramers doublet (red line), respectively. For this simulation the lowest two KDs were taken into account ( $4^6 = 4096$  microstates) instead of the lowest KD ( $2^6 = 64$  microstates;  $J_{12}/k_B = 4.89$  K).

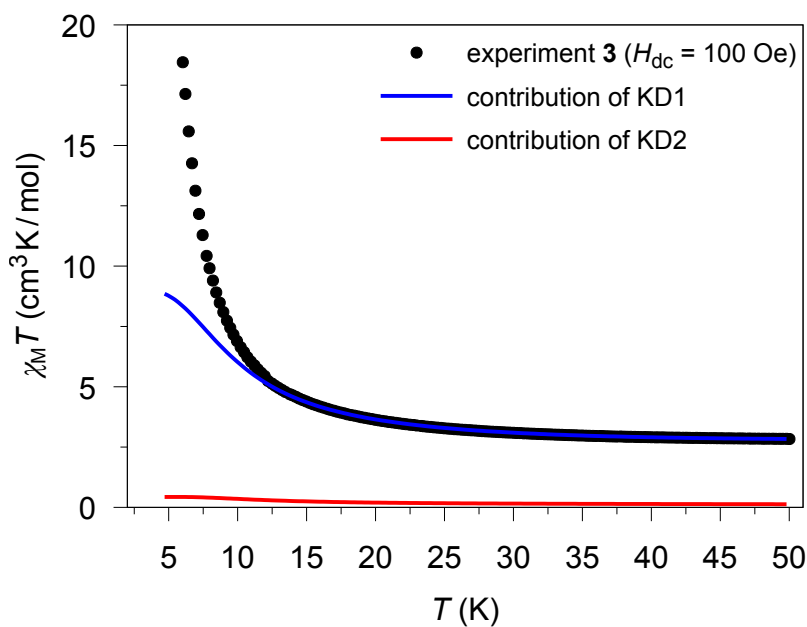


**Fig. S22:** Experimental ( $\bullet$ ) and calculated magnetic susceptibility  $\chi_M^{\text{calc}}(n=6)T$  of a six-membered spin ring for **3** (colored lines) decomposed into the contribution of the ground state Kramers doublet (blue line) and first excited Kramers doublet (red line), respectively. For this simulation the lowest two KDs were taken into account ( $4^6 = 4096$  microstates) instead of the lowest KD ( $2^6 = 64$  microstates;  $J_{12}/k_B \equiv J_{22}/k_B = 4.82$  K).